# Quick Compensation Method of Motor Phase Current Sensor Offsets without Motor Parameters for PMSM Drive

Koroku Nishizawa, Jun-ichi Itoh, and Yoshinobu Nishizawa,
Nagaoka University of Technology
Department of Electrical, Electronics and Information Engineering
Nagaoka, Niigata, Japan
koroku_nishizawa@stn.nagaokaut.ac.jp, itoh@vos.nagaokaut.ac.jp, yoshinobu_n@stn.nagaokaut.ac.jp

***Abstract*—This paper proposes a quick PMSM torque ripple reduction method caused by current sensor offsets. The proposed method consists of two novel offset compensation methods without any motor parameters. The first method estimates the current sensor offsets from output voltage references. Meanwhile, the second method estimates the current sensor offsets from detected output currents. By selecting the compensation method whose completion time of the compensation is shorter than the other under the different conditions of the PMSM drive, the quick compensation is achieved in the proposed method. It contributes to the application where the offsets vary in a short time, such as a HEV application. The effectiveness of the two compensation methods is confirmed by experiments. Moreover, it is confirmed that the completion time of the current sensor offset compensation is shortened by 12.0 seconds at most by accurately selecting one of two proposed methods of the current sensor offset compensation method.**

***Keywords—Current Sensor Offset Error Compensation, PMSM Drive.***

## I. INTRODUCTION

Recently, hybrid electric vehicles (HEVs) are rapidly becoming more common due to an increase in global environmental regulations. A HEV is an automobile that has an electric power train (EPT) added to its engine [1]-[10]. The EPT system consists of a battery, a voltage source inverter (VSI), and a permanent magnet synchronous motor (PMSM). The driving force of HEV is generated by the EPT. The motor torque ripple of the PMSM must be reduced in order to improve the riding quality of the HEV. There are several causes of the motor torque ripple, e.g. spatial harmonics of a permanent magnet flux of the PMSM, a dead-time of the VSI, and motor phase current sensor offsets.

Motor torque ripple reduction methods have been developed with focusing on the motor configurations [11]-[19]. In the solution with focusing on the motor configuration, an increase of the production cost for the motor is inevitable. Thus, approaches to the torque ripple reduction based on the motor control have also been considered. The torque ripple reduction methods which cancel out the effect of a dead-time of the VSI have been developed [20]-[22]. However, these methods cannot reduce the torque ripple caused by offsets of the motor phase currents. Generally, the motor current sensor offsets are compensated by adjusting the detected motor phase current values to zero during the motor is stopped, i.e. an off-line compensation method. However, the off-line compensation method cannot compensate the motor current sensor offsets, which dependently vary by the variation of temperature during the rotation of the motor.

So far, some on-line compensation methods have been proposed to compensate for the current sensor offsets during the drive of the motor with no motor parameters [23]-[26]. The methods in [23]-[24] compensate the motor current sensor offsets based on the output voltage references. Meanwhile, the method in [25] directly compensates the motor current sensor offsets based on the detected current values. In the HEV application, the current sensor offsets vary quickly due to the variation of the temperature because the load and speed of the PMSM are widely changed by the drive conditions. Therefore, the completion time of the current sensor offset compensation is required to be as short as possible. However, the completion time of the offset compensation has not been discussed yet. In particular, the completion time of each compensation method depends on the bandwidth of the current regulator in the PMSM drive system and the rotational speed. Thus, it is necessary to apply the compensation method whose the completion time of the compensation is shorter than the other under the different conditions of the PMSM drive.

This paper proposes the quick compensation method using two different compensation techniques in order to shorten the completion time of the compensation. At first, the two current sensor offset compensation methods in [23] and [25] are experimentally demonstrated. In addition, the completion time of the current sensor offset error compensation of the two methods are estimated by the simulation. Based on these results, by selecting the method whose completion time of the compensation is shorter than the other under particular conditions of the PMSM drive, the completion time of the compensation will be shortened.

## II. Torque Ripple Caused by Current Sensor Offset Error

Fig. 1 shows the general control block diagram for an IPMSM drive in the HEV. The current sensors are mounted into UVW-phases respectively. In order to simulate the effects of the current sensor offsets, the detected output phase current values ($i_{us}$, $i_{vs}$, $i_{ws}$) are obtained by intentionally adding the current sensor offsets ($i_{uoerr}$, $i_{voerr}$, $i_{woerr}$) to the true output phase current values ($i_{utr}$, $i_{vtr}$, $i_{wtr}$) as

$$\begin{aligned} i_{us} &= i_{utr} + i_{uoerr} \\ i_{vs} &= i_{vtr} + i_{voerr} \\ i_{ws} &= i_{wtr} + i_{woerr} \end{aligned} \quad (1).$$

In this paper, the errors in the gain of the current sensors are not considered and these gains are all regarded as 1.

The detected d-q- axis current values ($i_{ds}$, $i_{qs}$) are obtained as

$$\begin{aligned} i_{ds} &= i_{dtr} + i_{doerr} \\ i_{qs} &= i_{qtr} + i_{qoerr} \end{aligned} \quad (2),$$

by performing the transformation from three-phase to d-q rotational frame, where $i_{dtr}$ and $i_{qtr}$ are the true d-q- axis current values, whereas $i_{doerr}$ and $i_{qoerr}$ are the current sensor offset components in d-q- axis currents, respectively. Then, each term of (2) is expressed as

$$\begin{aligned} i_{dtr} &= \sqrt{\frac{2}{3}}\left\{ i_{utr}\cos\theta_e + i_{vtr}\cos\left(\theta_e - \frac{2\pi}{3}\right) + i_{wtr}\cos\left(\theta_e + \frac{2\pi}{3}\right)\right\} \\ i_{qtr} &= -\sqrt{\frac{2}{3}}\left\{ i_{utr}\sin\theta_e + i_{vtr}\sin\left(\theta_e - \frac{2\pi}{3}\right) + i_{wtr}\sin\left(\theta_e + \frac{2\pi}{3}\right)\right\} \\ i_{doerr} &= \sqrt{\frac{2}{3}}\left\{ i_{uoerr}\cos\theta_e + i_{voerr}\cos\left(\theta_e - \frac{2\pi}{3}\right) + i_{woerr}\cos\left(\theta_e + \frac{2\pi}{3}\right)\right\} \\ i_{qoerr} &= -\sqrt{\frac{2}{3}}\left\{ i_{uoerr}\sin\theta_e + i_{voerr}\sin\left(\theta_e - \frac{2\pi}{3}\right) + i_{woerr}\sin\left(\theta_e + \frac{2\pi}{3}\right)\right\} \end{aligned} \quad (3),$$

where $\theta_e$ is the electric angle.

In the general control system of the IPMSM, the detected d-q- axis current values shown in (2) is regulated to the d-q- axis current reference values ($i_d^*$, $i_q^*$ ) by the operation of the automatic current regulator (ACR). As a result, the true d-q- axis current values are transformed from (2) as

$$\begin{aligned} i_{dtr} &= i_{ds} - i_{doerr} = i_d^* - i_{doerr} \\ i_{qtr} &= i_{qs} - i_{qoerr} = i_q^* - i_{qoerr} \end{aligned} \quad (4).$$

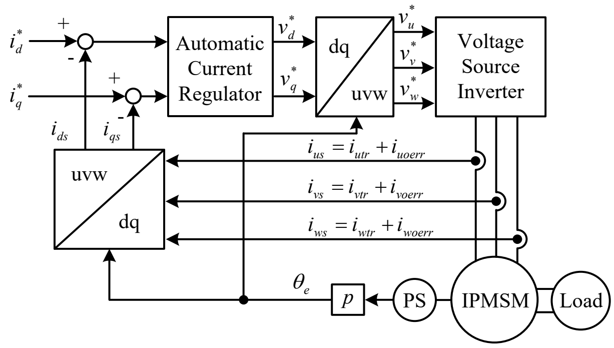


Fig. 1. General control block diagram for IPMSM drive in HEV.

Then, the torque of the IPMSM is calculated as

$$T = p\left\{\varphi_a i_{qtr} + (L_d - L_q) i_{dtr} i_{qtr}\right\} \quad (5),$$

where $p$ is the number of pole pairs, $\varphi_a$ is the magnet flux linkage, and $L_d$ and $L_q$ are the d-q- axis inductances, respectively. By substituting (3) and (4) to (5), the influence of the current sensor offsets for the motor torque can be observed by (6).

$$\begin{aligned} T &= p\left\{\varphi_a (i_q^* - i_{qoerr}) + (L_d - L_q)(i_q^* - i_{qoerr})(i_d^* - i_{doerr})\right\} \\ &= p\left\{\varphi_a i_q^* + (L_d - L_q) i_d^* i_q^*\right\} \\ &\quad + p\left\{(L_d - L_q)(-i_d^* i_{qoerr} - i_q^* i_{doerr} + i_{doerr} i_{qoerr}) - \varphi_a i_{qoerr}\right\} \end{aligned} \quad (6).$$

The first term of the right-hand side of (6) means the torque reference. The second term of the right-hand side of (6) means the torque ripple component caused by the current sensor offset error. The fundamental frequency of the torque ripple is the same as an electric angle frequency of the rotor position of the IPMSM.

## III. Compensation Methods For Current Sensor Offsets

### *A. Method I : Compensation for current sensor offsets by using output voltage references* [23]

Fig. 2 shows the control block diagram of the compensation method for the current sensor offsets by using output voltage references [23]. When the detected output phase currents have the current sensor offsets ($i_{uoerr}$, $i_{voerr}$, $i_{woerr}$), the voltage offsets occur in the output voltage references in order to cancel these sensor offsets, i.e. by the operation of the ACR. Therefore, the polarities of the current sensor offsets and the offsets in the voltage references ($v^*_{uoff}$, $v^*_{voff}$, $v^*_{woff}$) are opposite. The *method I* indirectly estimates the current sensor offsets from the voltage references by using this relationship.

Fig. 3 shows the calculation processes of the offsets from the voltage references. First, by applying discrete Fourier transform (DFT) to the inverter output voltage reference, the DC voltage reference is calculated as

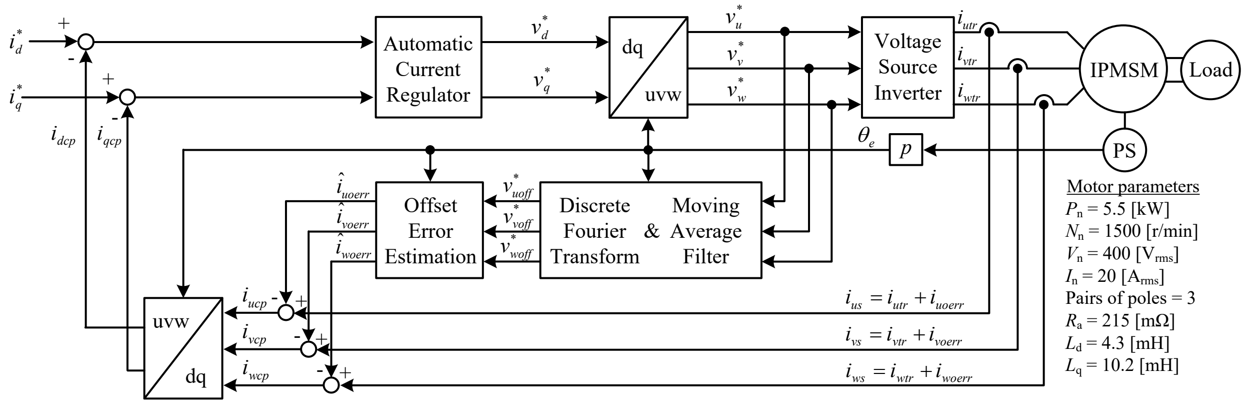


Fig. 2. Control block diagram of *method* I for compensating current sensor offsets by using output voltage references.

$$v_{udc}^{*} = \frac{\sum_{n}^{N_{sample}-1} v_{u}^{*}(n)}{N_{sample}} \tag{7}$$

where $N_{sample}$ is the number of sampling during one period of the electric angle frequency. Then, by applying the moving average filter (MAF) to the calculation results of (7), the offsets in the voltage references are calculated. The reason of using MAF is to suppress the variation of the calculation results of the offsets in the voltage references, which occur when the torque reference or the rotational speed reference is changed.

Fig. 4 shows the estimation process of the *method I* for the current sensor offsets. The current sensor offsets are estimated by subtracting the offsets in the voltage references, which is multiplied by an integral gain for the offset estimation, from the previous values of the estimated current sensor offsets as

$$\hat{i}_{uoerr} = \hat{i}_{uoerr.old} - \alpha \times v_{uoff}^{*} \tag{8}$$

where, $\alpha$ is the integral gain for the offset estimation. Finally, by subtracting the estimated current sensor offsets from the detected output phase current, the compensation for the current sensor offsets is finished.

### *B. Method II : Compensation for current sensor offsets by using detected output currents* [25]

Fig. 5 shows the control block diagram of the compensation method for current sensor offsets by using detected output currents. The *method II* directly estimates the current sensor offsets from the detected output currents by using the multistage DFTs.

Fig. 6 shows the estimation process of the *method II* for the current sensor offsets. By applying the multistage DFTs on the detected output phase currents, the current sensor offsets can be directly estimated from the detected output phase currents. The calculation process of each DFT is same as the *method I*, shown as (7).

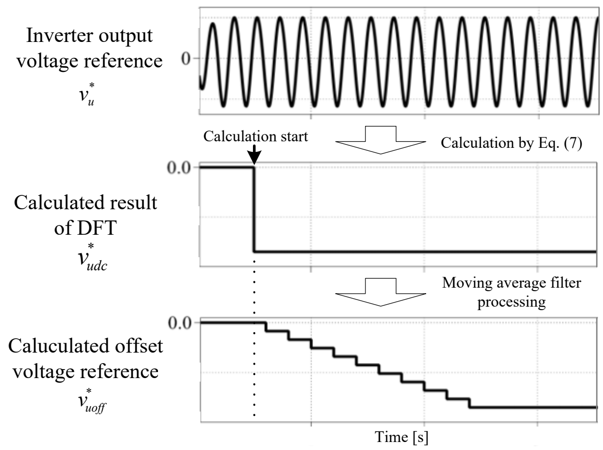


Fig. 3. Calculation processes for offset in voltage references.

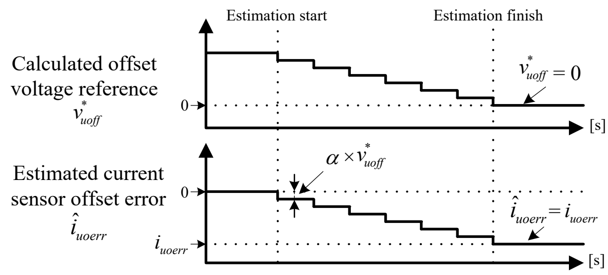


Fig. 4. Estimation process of *method I* for current sensor offsets.

## IV. Simulation and Experimental Results

Table I shows the motor parameters of the IPMSM for the test. In order to confirm the validities of the *method I* and *method II*, simulations are run under the same parameters.

Fig. 7 shows the simulation results of *method I* at the different rotational speeds. At the low rotational speed of 300 r/min., the completion time of the offset error compensation is 19 s. On the other hand, at high rotational speed of 750 r/min., the completion time is 8 s. in the high-speed region, the completion time is shorter than the completion time of 300 r/min.

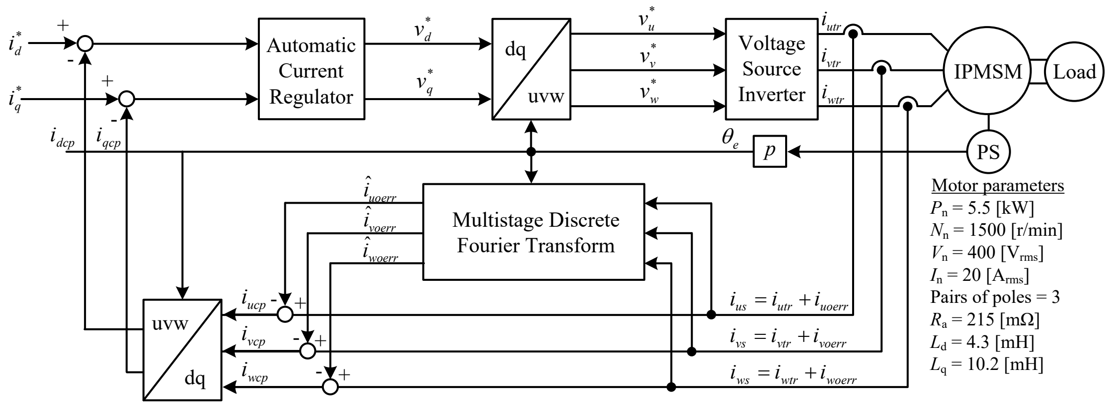


Fig. 5. Control block diagram of *method II* for compensating current sensor offsets by using detected output currents.

Fig. 8 shows the simulation results of *method II* at the different rotational speeds. At the low rotational speed of 300 r/min., the completion time of the offset error compensation is 5.5 s. On the other hand, at the high rotational speed of 750 r/min., the completion time is 14 s, longer than the completion time of 300 r/min. It is confirmed from Figs. 7 and 8 that the completion time of the offset error compensation of the *method I* and *method II* depend on the rotational speed. Furthermore, the completion time characteristics of the *method I* and *method II* are inversely related.

Fig. 9 shows the experimental results of the *method I* in steady state at a rotational speed ($N$) of 750 r/min, the angular frequency of ACR ($\omega_{ci}$) of 500 rad/s, a d-axis current command ($i_d^*$) of 0 A and-q- axis current command ($i_q^*$) of 4 A. The current sensor offsets are preset to $i_{uoerr}$ = 0.7 A, $i_{voerr}$ = 0.3 A, and $i_{woerr}$ = -1.0 A respectively and the integral gain for error estimation ($\alpha$) is 0.05. The current sensor offsets are estimated from the output voltage references and compensated. As a result, the torque ripple is reduced by 1.4 $Nm_{p\text{-}p}$ by applying the *method I*.

Fig. 10 shows the experimental results of the *method II* in a steady state at a rotational speed $N$ of 300 r/min, a $\omega_{ci}$ of 500 rad/s, a d-axis current command $i_d^*$ of 0 A and q-axis current command $i_q^*$ of 4 A. The current sensor offsets are preset to $i_{uoerr}$ = 1.0 A, $i_{voerr}$ = -0.6 A, and $i_{woerr}$ = -0.4 A, respectively. The current sensor offsets are estimated from the detected output currents and compensated. As a result, the torque ripple is reduced by 1.0 $Nm_{p\text{-}p}$ by applying the *method II*.

Fig. 11 shows the simulation results of the completion time of the offset compensation with two methods at the angular frequency of ACR ($\omega_{ci}$) of 500 rad/s. The horizontal axis of Fig. 9 is the ratio of the angular frequency of ACR to the electric angular frequency of the IPMSM ($\omega_e$). In the *method I*, the higher rotational speed is, the shorter the completion time of the offset error compensation becomes, because the repetition frequency of the estimation and compensation process, shown as Figs. 3 and 4, becomes higher when the rotational speed is high. On the other hand, the *method II* has an opposite characteristic of the completion time of the compensation against the rotational speed compared with the *method I*. The repetition frequency of the estimation process of the *method II*, shown as Fig. 9, also becomes higher when the rotational speed

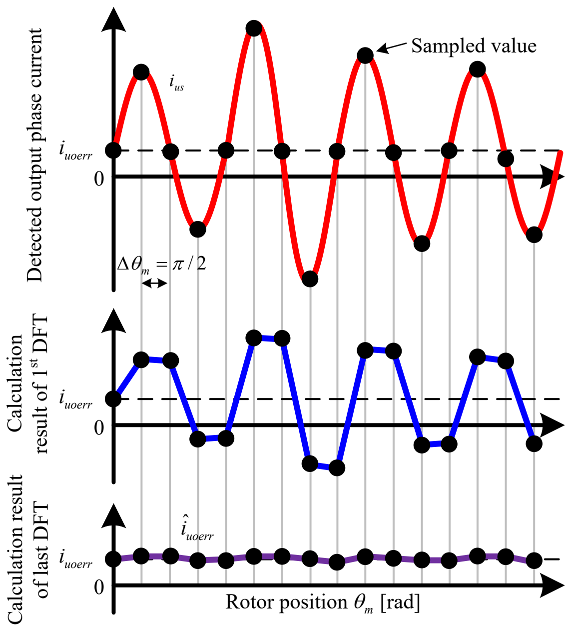


Fig. 6. Estimation processes of *method II* for current sensor offsets.

TABLE I. MOTOR PARAMETERS OF IPMSM AND SIMULATION AND EXPERIMENTAL CONDITIONS

| Symbol | Meaning | Value |
|---|---|---|
| $P_n$ | Rated motor power | 5.5 kW |
| $V_n$ | Rated voltage of motor | 400 $V_{rms}$ |
| $I_n$ | Rated current of motor | 20 $A_{rms}$ |
| $N_n$ | Rated rotational speed | 750 r/min. |
| $p$ | Number of pole pairs | 3 |
| $R$ | Winding resistance | 0.215 Ω |
| $L_d$ | *d*-axis inductance | 4.3 mH |
| $L_q$ | *q*-axis inductance | 10.2 mH |
| $\varphi_a$ | Back EMF constant | 0.284 V/rad/s |
| $i_d^*$ | *d*-axis current reference | 0 A |
| $i_q^*$ | *q*-axis current reference | 4 A |
| $i_{uoerr}$ | U-phase current sensor offset error | 0.7 A |
| $i_{voerr}$ | V-phase current sensor offset error | 0.3 A |
| $i_{woerr}$ | W-phase current sensor offset error | -1.0 A |
| $\omega_{ci}$ | Angular frequency of ACR | 500 rad/s |
| $\alpha$ | Integral gain of offset estimator in *method I* | 0.05 A/V |

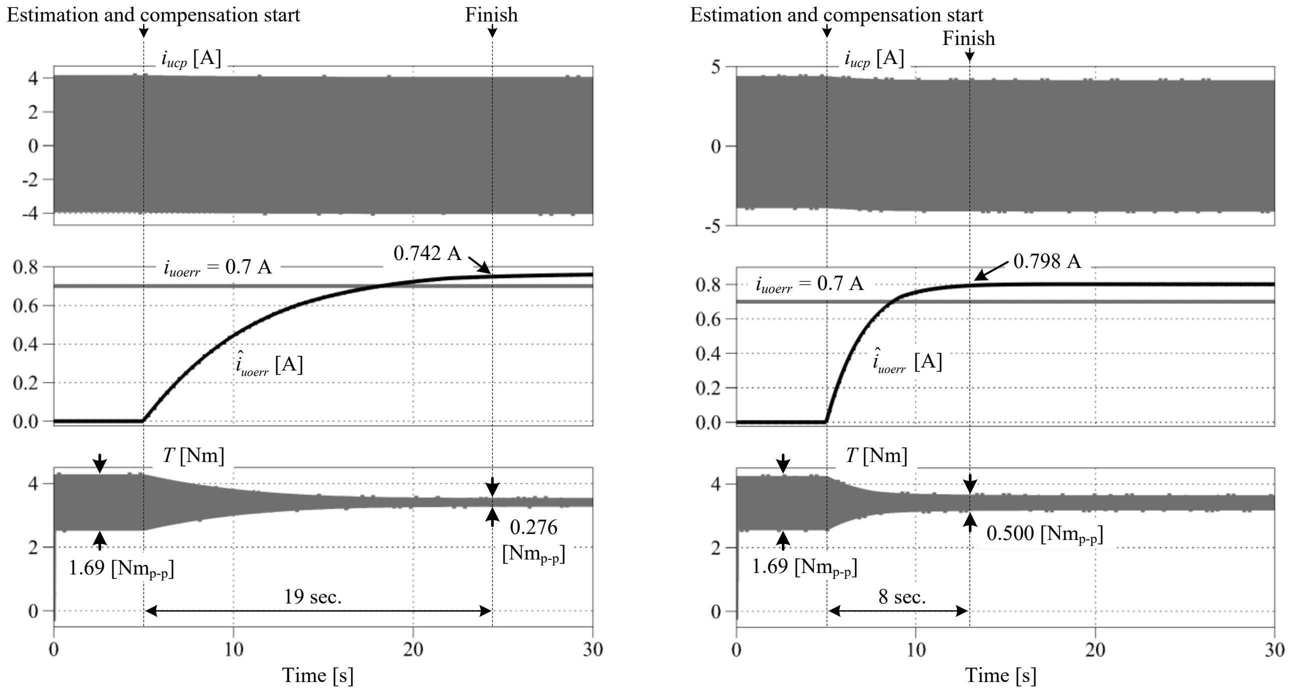


(a) $N = 300$ r/min. (b) $N = 750$ r/min.

Fig. 7. Simulation results of *method I* at different rotational speeds, $\omega_{ci} = 500$ rad/s, $i_d^* = 0$ A, $i_q^* = 4$ A, $i_{uoerr} = 0.7$ A, $i_{voerr} = 0.3$ A and $i_{woerr} = -1.0$ A. The integral gain for error estimation ($\alpha$) is 0.05.

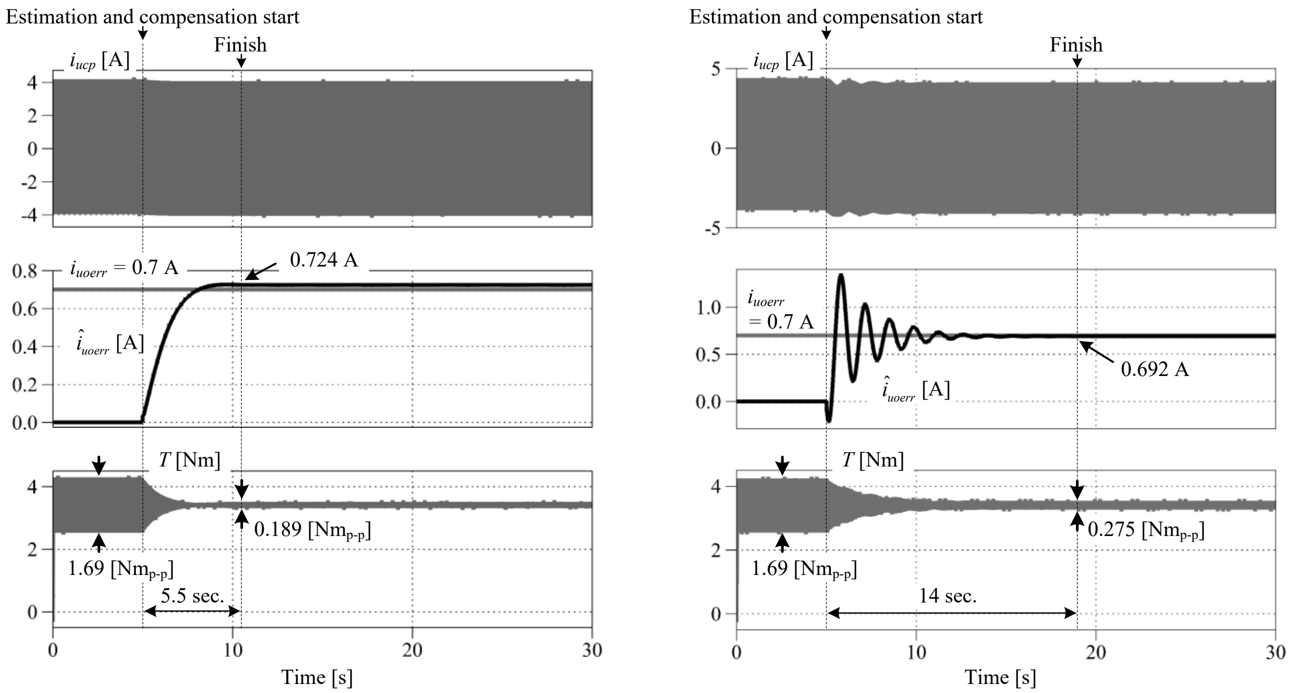


(a) $N = 300$ r/min. (b) $N = 750$ r/min.

Fig. 8. Simulation results of *method II* at different rotational speeds, $\omega_{ci} = 500$ rad/s, $i_d^* = 0$ A, $i_q^* = 4$ A, $i_{uoerr} = 0.7$ A, $i_{voerr} = 0.3$ A and $i_{woerr} = -1.0$ A.

is high. Furthermore, in the *method II*, the current sensor offsets are estimated directly from the detected current values. Therefore, when the rotational speed is high, the estimated values of the current sensor offsets oscillate and it takes a long time for the estimated values to converge. By selecting between the *method I* or *method II*, whose completion time of the compensation under the particular conditions of the PMSM drive is short, the completion time of the compensation is shortened by up to 12.0 s.

## V. CONCLUSION

In this paper, two compensation methods for the current sensor offset compensation without using the motor parameters are experimentally demonstrated. In addition, the completion times of the compensation of both methods were also assessed and compared by the simulation. By selecting the one of them, whose completion time of the compensation is shorter than the other depending on the particular conditions of the PMSM drive, the torque ripple caused by the current sensor offsets is quickly reduced. It was confirmed that the completion time was shortened up to 12.0 s by applying the proposed method. It will contribute the improvement of a riding quality of the HEV, because the proposed method quickly suppress the vibration caused by the torque ripple owing to the current sensor offsets depending on the temperature.

## REFERENCES


[1] J. M. Miller. "Power Electronics in Hybrid Electric Vehicle Applications," *Applied Power Electronics Conf. and Expo.*, Vol. 1, pp. 23-29 (2003).

[2] John M. Miller, "Hybrid Electric Vehicle Propulsion System Architectures of the e-CVT Type," *IEEE Trans. on Power Electronics*, Vol. 21, No. 3, pp. 756-767 (2006).

[3] S. S. Williamson, S. M. Lukic, and A. Emadi, "Comprehensive Drive Train Efficiency Analysis of Hybrid Electric and Fuel Cell Vehicles Based on Motor-Controller Efficiency Modeling," *IEEE Trans. on Power Electronics*, Vol. 21, No. 3, pp. 730-740 (2006).

[4] F. L. Mapelli, D. Tarsitano, and M. Mauri, "Plug-In Hybrid Electric Vehicle: Modeling, Prototype Realization, and Inverter Losses Reduction Analysis," *IEEE Trans. on Industrial Electronics*, Vol. 57, No. 2, pp. 598-607 (2010).

[5] Yuta Ikezawa, Hiroshi Fujimoto, Yoichi Hori, Daisuke Kawano, Yuichi Goto, Misaki Tsuchimoto, and Koji Sato, "Range Extension Autonomous Driving for Electric Vehicles Based on Optimal Velocity Trajectory Generation and Front-Rear Driving-Braking Force Distribution," *IEEJ Journal of Industry Applications*, Vol.5, No.3, pp.228-235 (2016).

[6] Kohei Aoyama, Naoki Motoi, Yukinori Tsuruta, and Atsuo Kawamura, "High Efficiency Energy Conversion System for Decreaces in Electric Vehicle Battery Terminal Voltage," *IEEJ Journal of Industry Applications*, Vol.5, No.1, pp.12-19 (2016).

[7] M. Arada, Y. Kurihara, D. Misu, M. Matsubara, "EV and HEV Motor Development in TOSHIBA," *IEEJ Journal of Industry Applications*, Vol. 4, No. 3, pp. 152-157 (2015).

[8] Y. Hosoyamada, M. Takeda, T. Nozaki, N. Motoi, A. Kawamura, "High Efficiency Series Chopper Power Train for Electric Vehicles Using a Motor Test Bench," *IEEJ Journal of Industry Applications*, Vol. 4, No. 4, pp. 460-468 (2015).

[9] A. Sciarretta, M. Back and L. Guzzella, "Optimal control of parallel hybrid electric vehicles," *IEEE Trans. on Control Systems Technology*, Vol. 12, No. 3, pp. 352-363 (2004).

[10] C. C. Chan and Y. S. Wong, "Electric vehicles charge forward", *IEEE Power and Energy Magazine*, Vol. 2, No. 6, pp. 24-33 (2004).

[11] G. H. Kang, Y. D. Son, G. T. Kim, and J. Hur, "A Novel Cogging Torque Reduction Method for Interior-Type Permanent-Magnet Motor," *IEEE Trans. Ind. Appl.*, Vol. 45, No. 1, pp. 161-167 (2009).

[12] T. M. Jahns, and W. L. Soong, "Pulsating Torque Minimization Techniques for Permanent Magnet AC Motor Drives-a review," *IEEE Trans. Ind. Appl.*, Vol. 32, No. 2, pp. 321-330 (1996).


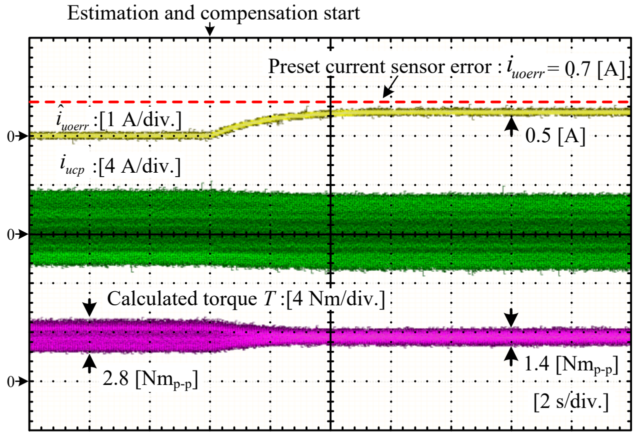


Fig. 9. Estimation of current sensor offsets and reduction of motor torque ripple with *method I* in steady state at $N$ = 750 r/min, $\omega_{ci}$ = 500 rad/s, $i_d^*$ = 0 A, $i_q^*$ = 4 A, $i_{uoerr}$ = 0.7 A, $i_{voerr}$ = 0.3 A and $i_{woerr}$ = -1.0 A. The integral gain for error estimation ($\alpha$) is 0.05.

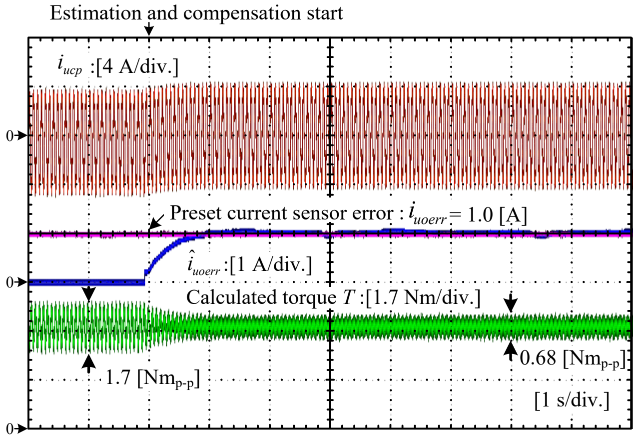


Fig. 10. Estimation of current sensor offset error and reduction of motor torque ripple with *method II* in steady state at $N$ = 300 r/min, $\omega_{ci}$ = 500 rad/s, $i_d^*$ = 0 A, $i_q^*$ = 4 A, $i_{uoerr}$ = 1.0 A, $i_{voerr}$ = -0.6 A and $i_{woerr}$ = -0.4 A.

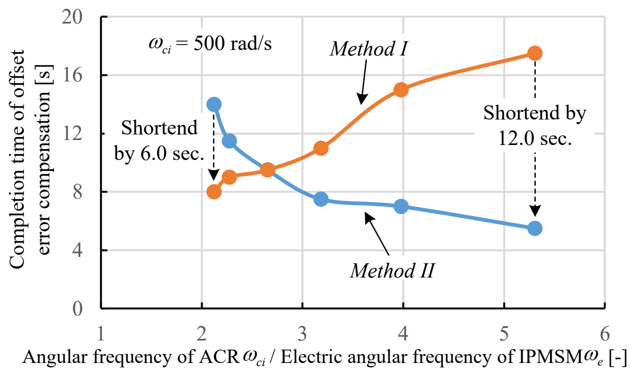


Fig. 11. Completion time of offset error compensation of *method I* and *method II* under different condition of rotational speed. The angular frequency of ACR ($\omega_{ci}$) is 500 rad/s.

[13] Satoshi Imamori, Hideki Ohguchi, Masao Shuto, and Akio Toba, "Relation between Magnetic Properties of Stator Core and Cogging Torque in 8-pole 12-slot SPM Synchronous Motors," *IEEJ Journal of Industry Applications*, Vol.4, No.6, pp.696-702 (2015).

[14] Jef Beerten, Jan Verveckken, and Johan Driesen, "Predictive Direct Torque Control for Flux and Torque Ripple Reduction," *IEEE Trans. on Industrial Electronics*, Vol. 57, No. 1, pp. 404-412 (2010).

[15] Y. Yokoi, T. Higuchi, "Selective Elimination of EMF Harmonics with Stepped Skewing for Ripple Torque Reduction in Surface-Mounted Permanent Magnet Motors," *IEEJ Journal of Industry Applications*, Vol, 3, No. 6, pp. 463-469 (2014).

[16] E. Levi, "Multiphase Electric Machines for Variable-Speed Applications" *IEEE Transactions on Industrial Electronics*, Vol. 55, No. 5, pp. 1893-1909 (2008).

[17] K. Park, J. H. Lee, Y. J. Kim, S. Y. Jung, "A novel torque ripple reduction method for IPMSM using asymmetric notch lamination design," *19th International Conference on Electrical Machines and Systems* (ICEMS 2016), pp. 1-4 (2016).

[18] M. Suzuki and K. Sakai, "Reduction of torque ripple for PM motor with toroidal winding," *19th International Conference on Electrical Machines and Systems* (ICEMS 2016), pp. 1-6 (2016).

[19] V. Bilyi, D. Gerling and D. Bilyi, "Flux barrier design method for torque ripple reduction in synchronous reluctance machines," *IEEE Transportation Electrification Conference and Expo, Asia-Pacific* (ITEC Asia-Pacific 2016, pp. 34-39 (2016).

[20] H. S. Kim, H. T. Moon, and M. J. Youn, "On-line Dead-time Compensation Method Using Disturbance Observer," *IEEE Trans. Power Electron.*, Vol. 18, No. 6, pp. 1336-1345 (2003).

[21] N. Urasaki, T. Senjyu, K. Uezato, and T. Funabashi, "An Adaptive Dead-Time Compensation Strategy for Voltage Source Inverter Fed Motor Drives," *IEEE Trans. Power Electron.*, Vol. 20, No. 5, pp. 1150-1160 (2005).

[22] Shuhei Shimmyo, Kazuaki Yuki, and Kouhei Ohnishi,”Torque Ripple Suppression Method with Multilevel Inverter and Feedforward Dead-Time Compensation”,IEEJ J. Industry Applications, vol.5, no.4, pp.36-369, 2016.

[23] H. Tamura, T. Ajima, and Y. Noto, "A Torque Ripple Reduction Method by Current Sensor Offset Error Compensation," *EPE 2013*, pp. 1-10 (2013).

[24] Myoungho Kim, Seung-Ki Sul, and Junggi Lee, "Compensation of Current Measurement Error for Current-Controlled PMSM Drives," *IEEE Trans. Ind. Appl.*, Vol. 50, No. 5, pp. 3365-3373 (2014).

[25] H. Tamura, T. Ajima, Y. Noto, and J. Itoh, "A Novel Compensation Method for a Motor Phase Current Sensor Offset Error Varied during a VSI-Motor Drive," *IPEC2014*, pp. 682-688 (2014).

[26] H. Tamura, J. Itoh and Y. Noto, "Two methods for compensating motor-current-sensor offset error by using DC-voltage component included in phase-voltage command for current-controlled PMSM drive," *17th European Conference on Power Electronics and Applications* (EPE'15 ECCE-Europe) 2015, pp. 1-10 (2015).